Drug Design, Development and Therapy

Dovepress
Taylor & Francis Group

Open Access Full Text Article

ORIGINAL RESEARCH

Potential of Sivelestat for Pulmonary Arterial Hypertension Treatment: Network Pharmacology-Based Target Identification and Mechanistic Exploration

Xiaodong Deng[1], Pengcheng Qiu[2], Xin Li[2], Yukun Hu[1], Qing Que[1], Kunchi Zhang[1], Tianlin Deng[1], Yi Liu[1]

[1]Department of Critical Care Medicine, Panzhihua Central Hospital, Panzhihua, 61700, People's Republic of China; [2]Department of Cardiothoracic Surgery, The First Affiliated Hospital, Jinzhou Medical University, Jinzhou, 121000, People's Republic of China

Correspondence: Yi Liu, Email yi603915991@163.com

Background: Sivelestat is a specific neutrophil elastase inhibitor that is currently approved for the treatment of acute lung injury and acute respiratory distress syndrome. Given sivelestat's established anti-inflammatory and antioxidant properties, its efficacy in treating pulmonary arterial hypertension (PAH) remains uncertain. This study aims to investigate the potential of sivelestat as a treatment for PAH.

Methods: Sivelestat's effects on PAH were evaluated using hypoxia-induced rat models (10% O_2, 4 weeks) and pulmonary arterial endothelial/smooth muscle cells (1% O_2). Rats received sivelestat (20–100 mg/kg) for 2 weeks, with hemodynamic (RVSP) and vascular remodeling (%WT) assessments. In vitro, sivelestat (50–200 μM) suppressed hypoxia-driven proliferation (CCK-8, EdU), migration (Transwell), and angiogenesis. Molecular validation via qPCR/Western blot confirmed reduced expression of key targets (IGF1R, JAK1, JAK2, PDGFRB).

Results: Through predictive analysis, we identified 595 potential genes associated with sivelestat in the treatment of PAH. Notably, ERBB2, IGF1R, JAK1, JAK2, PDGFRB, and PTPN11 emerged as key hub genes. In vivo experiments demonstrated that administration of sivelestat at a dose of 100 mg/kg significantly reduced PAH and improved pulmonary vascular remodeling. In vitro experiments indicated that sivelestat effectively decreased the proliferation and migration of PAECs and PASMCs induced by hypoxia.

Conclusion: Sivelestat has the potential to treat PAH through various targets and pathways. We have initially elucidated the molecular mechanism by which sivelestat acts in the treatment of PAH and have conducted preliminary validation through molecular docking studies and experimental approaches.

Keywords: network pharmacology, pulmonary artery hypertension, sivelestat, molecular dynamic

Introduction

PAH is a severe condition characterized by elevated blood pressure in the pulmonary arteries, leading to significant morbidity and mortality.[1] Epidemiological studies estimate that the prevalence of PAH is approximately 15–50 cases per million population, with varying incidence based on underlying causes such as idiopathic PAH, connective tissue diseases, and left heart diseases.[2,3] The pathogenesis of PAH is multifactorial, involving complex molecular regulatory networks that include vascular remodeling, inflammation, and endothelial dysfunction.[4,5] Current treatment options include vasodilators, endothelin receptor antagonists, and phosphodiesterase-5 inhibitors;[6] however, many patients remain symptomatic, underscoring the need for new therapeutic strategies. Given the intricate nature of molecular pathways involved in PAH, there is an urgent demand for novel pharmacological agents that target these mechanisms, ultimately improving patient outcomes and quality of life.

Received: 30 November 2024
Accepted: 4 May 2025
Published: 20 May 2025

Emerging evidence implicates neutrophil elastase (NE) in PAH progression,[7] where it promotes vascular remodeling by degrading extracellular matrix components, activating pro-inflammatory cytokines, and inducing endothelial dysfunction.[8] Elevated NE levels correlate with disease severity in PAH patients,[9] making it a compelling therapeutic target. As a specific NE inhibitor, sivelestat has demonstrated efficacy in reducing vascular injury and inflammation in preclinical models of acute lung injury and sepsis[10,11] Critically, recent studies highlight NE's role in driving pulmonary artery smooth muscle cell (PASMC) proliferation and endothelial apoptosis,[12,13] processes central to PAH pathogenesis. By inhibiting NE, sivelestat may disrupt these pathways, offering a novel mechanism to ameliorate PAH. Existing PAH therapies (eg, vasodilators, endothelin antagonists) primarily target hemodynamic abnormalities but inadequately address vascular remodeling.[6] Sivelestat's dual action—suppressing inflammation and directly inhibiting vascular cell proliferation[13]—positions it as a promising candidate to fill this therapeutic gap. Network pharmacology is a novel approach that integrates systems biology and pharmacology, allowing researchers to explore the interactions between drugs, targets, and diseases.[14] Introduced in the early 2000s, this methodology emphasizes the complexity of biological systems and the multifactorial nature of diseases.[14] Network pharmacology facilitates drug discovery by identifying potential therapeutic targets and predicting drug interactions while considering the interconnectedness of biological pathways.[15] It has been instrumental in researching various drugs, including those for cancer and cardiovascular diseases.[15,16] This study aims to utilize network pharmacology to elucidate the potential targets and biological mechanisms of sivelestat in the treatment of PAH, thus providing insights into its therapeutic relevance for this complex disease. The flowchart of the research is shown below (Figure 1).

Materials and Methods

Screening Potential Targets for Sivelestat and PAH

Potential targets of Sivelestat were identified using multiple databases, including PharmMapper (Reverse pharmacophore matching to identify targets based on 3D ligand structures. Parameters: Fit score threshold: ≥3.0 (default for high-confidence

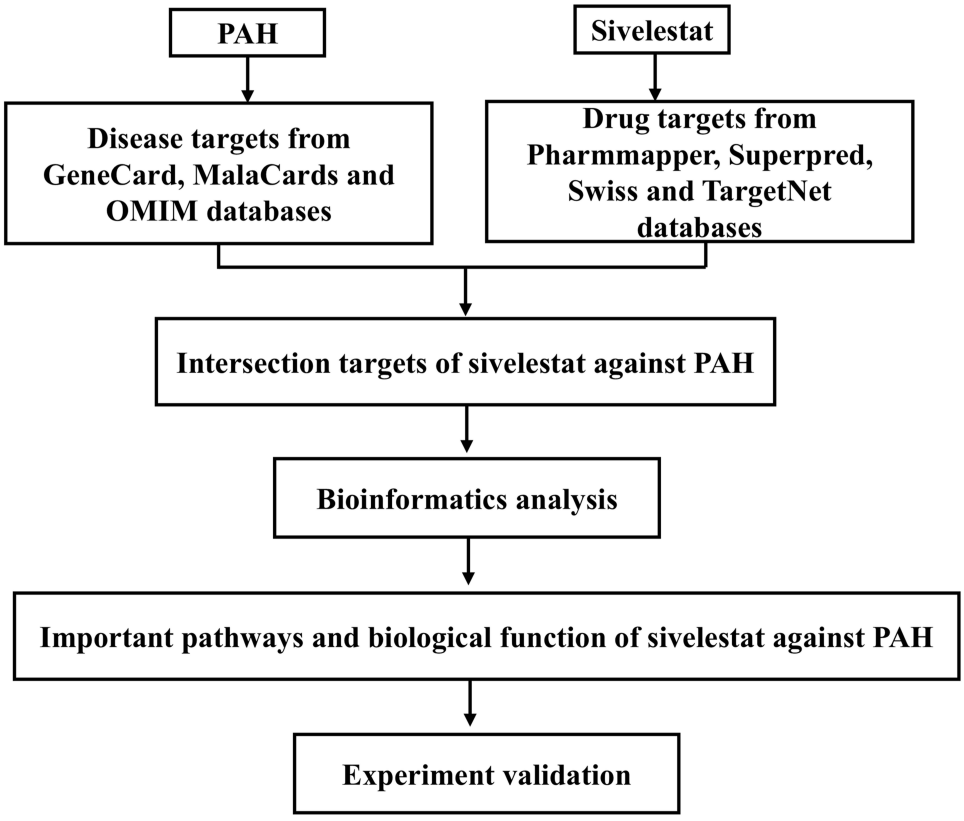

Figure 1 Flowchart of Network Pharmacology Research.

predictions).[17] SuperPred (Similarity-based ligand-target prediction using the Similarity Ensemble Approach (SEA). Parameters: Tanimoto coefficient cutoff: ≥0.7 (to ensure structural similarity).[18] Swiss (Machine learning-based prediction using ligand 2D/3D descriptors. Parameters: Probability threshold: ≥20% (default for moderate-to-high confidence).[19,] and TargetNet (Deep learning model trained on ChEMBL bioactivity data. Parameters: Probability cutoff: ≥0.5 (balanced precision-recall).[20,] After integrating these targets, duplicates were removed to establish the relevant targets for Sivelestat. Subsequently, pathogenic targets associated with PAH were extracted from the GeneCard,[21] Malacard,[22] and OMIM databases.[23,] Following the elimination of duplicate targets, the remaining entries were considered pertinent to PAH. Both Sivelestat and PAH targets were standardized to their official gene symbols using the UniProt database.[24] A Venn diagram was utilized to identify the intersection of genes between the targets of Sivelestat and those associated with PAH.[25,]

Construction of a Protein–Protein Interaction (PPI) Network

The String database is a tool designed for analyzing PPI.[26] In this study, we imported the intersection genes into the String database and utilized the settings specific to Homo sapiens for our analysis. We established a confidence score threshold of greater than 0.9 and opted to hide disconnected nodes, thereby generating the gene PPI network for further analysis.

Cluster Analysis of Hub Genes

After conducting an in-depth analysis of PPI data, we utilized the MCODE and Cytohubba plug-ins within Cytoscape software to generate node clusters and identify central nodes,[27,28] respectively. The MCODE plug-in is specifically designed to identify clusters of nodes that share similar biological functions, with the node exhibiting the highest score in each cluster referred to as a SEED, which is regarded as a key target for that particular cluster. Additionally, the Cytohubba plug-in offers 11 different topological analysis methods to rank the nodes in the PPI network based on their characteristics,[29] with the goal of identifying hub genes among them. To enhance the credibility of our recognition results, we employed a variety of evaluation methods, particularly four algorithms: Degree (Number of direct interactions), Maximal Clique Centrality (MCC, Nodes in the largest fully connected subnetwork), Edge Percolated Component (EPC, Resilience to edge removal), and Density of Maximum Neighborhood Component (DMNC, Local network density) to pinpoint important genes.[29,30] The common genes identified among the top 50 genes selected based on these four topological analysis methods were classified as hub genes. Final Hub Genes: ERBB2, IGF1R, JAK1, JAK2, PDGFRB, PTPN11 were prioritized as they ranked in the top 50 across all four algorithms.

GO and KEGG Pathway Enrichment Analyses

The functional enrichment analysis tool, OmicShare, is a free online data analysis platform designed for conducting GO and KEGG pathway enrichment analyses.[31] In the GO analysis, significant enrichment of genes was observed across three categories: biological process (BP), cellular component (CC), and molecular function (MF). Concurrently, the KEGG pathway analysis identified key signaling pathways associated with the studied genes. A q-value-adjusted significance level was employed in this analysis, with a critical threshold set at $p < 0.05$.

Molecular Docking

The binding of sivelestat sodium to its target was thoroughly analyzed using AutoDock Vina software.[32] Initially, we acquired the three-dimensional crystal structures of six key genes from the Protein Data Bank (PDB).[33,] Subsequently, the three-dimensional structure of sivelestat sodium was retrieved from the PubChem database,[34] and its format was converted into a PDB file using OPEN Babel software.[35] Finally, molecular docking of the core compound and the target was performed with AutoDock 4, and the results were visualized using Pymol software. An affinity value of less than 6.5 kcal/mol indicates effective binding between the compound and the target.

Molecular Dynamics Simulations

100ns molecular dynamics simulations (MD) of the complexes were performed using Gromacs 2022 software. Charmm 36[36] was chosen as the protein force field, Gaff2 was chosen as the ligand force field, the TIP3P water model was chosen to add solvents to the protein-ligand system and to create a water box with a periodic boundary

 https://doi.org/10.2147/DDDT.S507240

of 1.2 nm.[37] The particle grid Ewald (PME) and Verlet algorithms are used to deal with electrostatic interactions respectively. Then 100,000 steps of isothermal isovolumetric ensemble equilibrium and isothermal isobaric ensemble equilibrium were simulated with a coupling constant of 0.1 ps and a duration of 100 ps. Both van der Waals and Coulomb interactions are calculated using 1.0 nm cutoff values. Finally, the system was simulated using Gromacs 2022 at constant temperature (310 K) and constant pressure (1 bar) for a total of 100 ns.

Animal Experiments

Prior to euthanizing the rats, we first anesthetized them by administering an intraperitoneal injection of sodium pentobarbital at a dosage of 40 mg/kg. Subsequently, a PE-50 catheter (Taimeng, Chengdu, China), preloaded with copper heparin, was inserted into the right ventricle via the right external jugular vein. The opposite end of the catheter was connected to a pressure transducer (Taimeng, Chengdu, China) and linked to a multiconductor physiological recorder to measure right ventricular systolic pressure (RVSP, in mm Hg). The recorded RVSP values can indirectly reflect changes in pressure within the pulmonary artery. Following the removal of heart and lung tissues, we immersed these specimens in paraformaldehyde and conducted hematoxylin and eosin staining to assess the remodeling of both the right ventricle and the pulmonary artery. We then calculated the percentage of mid-layer wall thickness (WT%) using the formula: WT% = 2 × (WT/external diameter) × 100.

Dosing Schedule of Sivelestat

We evaluated the therapeutic effects of sivelestat on PAH through animal experiments. After establishing the pulmonary arterial hypertension (PAH) model in rats through four weeks of hypoxic exposure, the animals received sivelestat administration for an additional two weeks. Hypoxic rats received daily intraperitoneal injections of sivelestat. The dosages of sivelestat (20 mg/kg/d, 50 mg/kg/d, and 100 mg/kg/d) were established based on findings from prior studies.[38]

Establishment of a Rat Model of Hypoxia-Induced PAH

In this study, we utilized 6 to 8-week-old male Sprague-Dawley (SD) rats, all of which were sourced from Jinzhou Medical University and were in good health. The rats were housed under standard conditions with unrestricted access to food and water. All animal experiments and procedures were approved by the Research Ethics Committee of Jinzhou Medical University (Approval Number: 2022031001). Following a 7-day acclimation period, the research team placed the hypoxic model rats in an environment equipped with a gas-controlled delivery system (Oxycycler Model A84XOV; BioSpherix, Ltd., China), where the oxygen concentration was maintained at 10% ± 0.5%. In contrast, the male rats in the control group were raised under normal oxygen conditions (21% O2). To ensure that the carbon dioxide concentration in the laboratory remained below 3%, soda lime was placed in the chamber to absorb CO2, while color-changing silica gel was employed to absorb water vapor. After 4 weeks of hypoxic exposure, we administered treatments to the rats via intraperitoneal injection of sivelestat or saline. Throughout the experiment, all rats were maintained in an environment with temperatures ranging from 23°C to 26°C, following a 12-hour light and dark cycle. The health status and behavior of the animals were monitored weekly to ensure the smooth progress of the experiment, and no rats died prior to the conclusion of the study.

Measurement of Distance Traveled

To evaluate the exercise capacity of the rats, their maximum running distance on a treadmill was measured. The test commenced with the treadmill belt set at an initial speed of 10 m/min, which increased by 5 m/min every 5 minutes until reaching a maximum speed of 25 m/min. This maximum speed was then maintained for 15 minutes. The test concluded either after 30 minutes or when the rat exhibited signs of fatigue, defined as a lack of movement for more than 5 seconds on the shock grid. This study adhered to ethical standards for animal experiments.

Cell Culture

PAECs (Catalog #3100) and PASMCs (Catalog, #3110) were obtained from Sciencell Company and cultured in specialized media (Cat. #1001, #1101). Cells from passages 3 to 6 were selected for subsequent experiments. To further

investigate the potential mechanism of sivelestat in the treatment of PAH, both cell types were subjected to a hypoxic environment (1% O2) and cultured for 24 hours. Concurrently, we assessed the effects of sivelestat treatment on cell migration and proliferation. The concentrations of sivelestat administered were 50 μmol/L, 100 μmol/L, and 200 μmol/L, which were selected based on findings from previous studies.[38]

Quantitative PCR (qPCR)

Total RNA was extracted from pulmonary artery endothelial tissue using Trizol reagent (Invitrogen), following the manufacturer's instructions. After extraction, 2 μg of total RNA was reverse transcribed into cDNA using a reverse transcription kit (Transgene). Subsequently, qPCR analysis was conducted using SYBR Green PCR mix (Beyotime, China) and a real-time PCR instrument (ABI 7500). CT values were obtained through the Applied Biosystems 7500 sequence detection system software, with β-actin serving as an internal reference to ensure the accuracy of the results. All primers were designed by Primerbank and synthesized by Sangon Biotech (shanghai, China).

Western Blotting

After carefully peeling the pulmonary artery from the rat lung tissue, use forceps to cut the artery and scrape the endothelial tissue. The endothelial tissue was lysed in a mixture of RIPA lysis buffer and protease inhibitors. Following Bicinchoninic Acid quantification, samples containing 30 μg of protein were separated on a 10% SDS-PAGE gel and subsequently transferred to a polyvinylidene difluoride (PVDF) membrane. After blocking with 5% bovine serum albumin, the PVDF membrane was incubated with primary antibodies for 12 hours at 4°C, followed by a 2-hour incubation with secondary antibodies from the corresponding species. After the addition of Enhanced Chemiluminescence luminescent solution, the protein bands were imaged using a chemiluminescence system. Data were quantitatively analyzed using ImageJ, with β-actin serving as the loading control. The corresponding primary antibodies are listed as follows: Insulin-like growth factor 1 receptor (IGF1R, ab182408, 1:1000, Abcam), Erb-b2 receptor tyrosine kinase 2 (ERBB2, ab134182, 1:1000, Abcam), Janus kinase 1 (JAK1, ab133666, 1:5000, Abcam), Janus kinase 2 (JAK2, ab108596, 1:5000, Abcam), Platelet derived growth factor receptor beta (PDGFRB, ab313777, 1:1000, Abcam), Protein tyrosine phosphatase non-receptor type 11 (PTPN11, ab300579, 1:1000, Abcam), Actin beta (β-actin, ab7817, 1:1000, Abcam).

Cell Proliferation Assay

We utilized the CCK-8 test kit (K1076l; APExbio, USA) to assess cell viability. Specifically, different groups of PAECs and PASMCs were seeded into 96-well plates. After six hours of incubation, the plates were subjected to either normal oxygen conditions or hypoxic conditions for an additional 24 hours. At the conclusion of the 24-hour incubation period, we added 10 μL of CCK-8 solution to each well and incubated the plates at 37°C for 1.5 hours. Subsequently, the absorbance of each well was measured using a microplate reader at a wavelength of 450 nm. Additionally, we employed the 5-Ethynyl-2′-deoxyuridine (Edu) cell proliferation assay kit (K1076l; APExbio) to evaluate the proliferation of PAECs and smooth muscle cells, adhering to the manufacturer's instructions. In this study, these cells were cultured in six-well plates under both normoxic and hypoxic conditions. Each well was seeded with 5 × 10^4 cells and incubated at 37°C for 3 hours following the addition of 1 mL of Edu to each group. To fix the cells, we added 4% paraformaldehyde for 20 minutes and subsequently incubated each well with 0.5 mL of click reaction solution for 30 minutes. To ensure the reliability of the experimental results, the entire experiment was repeated at least four times. Finally, we stained the nuclei with DAPI for 10 minutes to facilitate visualization and subsequent analysis.

Cell Migration Assay

Cell migration was assessed using Transwell and scratch assays. In the scratch assay, cells from different groups were seeded onto a 6-well culture plate at a density of 5 × 10^5 cells per well and cultured until confluence was achieved. A clean 200 μL pipette tip was then used to create a linear scratch on the surface of the wells. Following this, the cells were washed three times with PBS, and serum-free medium was added before culturing under appropriate conditions for 24 hours. Migration width was measured using an inverted optical microscope (IX71, Olympus Corporation, Japan), and

images were captured at 0 and 24 hours. For the Transwell assays, 24-well plates were utilized according to the manufacturer's instructions. In this setup, 200 μL of FBS-free cell suspension, containing a total of 10,000 cells, was placed in the upper chamber, while 600 μL of FBS-containing medium (without cells) was added to the lower chamber. After co-incubation for 24 hours, the upper chamber was removed, and the cells were fixed with 4% paraformaldehyde. Subsequently, cells were stained with 1% crystal violet solution for 15 minutes, and non-migrated cells on the upper surface of the membrane were gently wiped away using a cotton swab. Finally, the migrating cells were photographed using an optical microscope to document the experimental results.

Statistical Analysis

Sample sizes were determined a priori using power analysis (G*Power 3.1, $\alpha = 0.05$, power = 0.8, effect size derived from pilot experiments), resulting in n = 8 rats per group (Four deaths occurred in the hypoxia model group) for in vivo studies and n = 4 independent biological replicates for in vitro assays. Data are expressed as mean ± standard deviation (SD). Normality was assessed using the Shapiro–Wilk test, and homogeneity of variance was confirmed via Levene's test. For comparisons between two groups, an unpaired two-tailed Student's *t*-test was applied to normally distributed data; non-parametric Mann–Whitney *U*-tests were used otherwise. Multi-group analyses employed one-way ANOVA with Tukey's post hoc correction for normally distributed data or Kruskal–Wallis with Dunn's test for non-parametric datasets. All analyses were performed using GraphPad Prism 9.0 (GraphPad Software, USA), with statistical significance set at $P < 0.05$. Experimental protocols were independently replicated four times to ensure reproducibility.

Results

Identification of Targets of Sivelestat and PAH

Identification of sivelestat and targets for PAH. We examined the 2D structure of sivelestat using the ZINC database (Figure 2A). Following this, we searched the PharmMapper, SuperPred, Swiss, and TargetNet databases, removing duplicates, which resulted in the identification of 746 genes as potential targets of sivelestat. To gather pathogenic genes associated with PAH, we utilized the GeneCard, MalaCards, and OMIM databases. After eliminating duplicates, 7383 genes were identified as candidate pathogenic genes. By intersecting these with the previously identified potential targets of sivelestat, we obtained 595 potential targets for sivelestat in the treatment of PAH (Figure 2B). Subsequently, we employed the OmicShare online platform to conduct GO enrichment analysis and KEGG signaling pathway analysis on these 595 genes to elucidate the possible mechanisms by which sivelestat may treat PAH. The top 20 KEGG signaling pathways, ranked by q-value, along with the top 8 BP, CC, and MF terms, were visualized using histograms. The analysis of the top ten KEGG signaling pathways is presented in the figure These pathways include: Neuroactive ligand-receptor interaction, Calcium signaling pathway, cAMP signaling pathway, Prostate cancer, PI3K-Akt signaling pathway, Lipid and atherosclerosis, Pancreatic cancer, Non-small cell lung cancer, AGE-RAGE signaling pathway in diabetic complications, and EGFR tyrosine kinase inhibitor resistance (Figure 2C). The first eight BP terms encompass the adenylate cyclase-modulating G protein-coupled receptor signaling pathway, vascular processes within the circulatory system, regulation of tube diameter, maintenance of blood vessel diameter, regulation of tube size, response to xenobiotic stimuli, positive regulation of cytosolic calcium ion concentration, and response to lipopolysaccharide. Related CC terms include membrane rafts, membrane microdomains, integral components of the presynaptic membrane, synaptic membranes, neuronal cell bodies, intrinsic components of the presynaptic membrane, integral components of synaptic membranes, and intrinsic components of synaptic membranes. Related MF terms encompass G protein-coupled peptide receptor activity, protein tyrosine kinase activity, and peptide receptor activity, nuclear receptor activity, ligand-activated transcription factor activity, neurotransmitter receptor activity, protein serine/threonine kinase activity, G protein-coupled amine receptor activity (Figure 2D).

The Binding Affinity between Sivelestat and Hub Genes was Confirmed Through Molecular Docking Studies

To identify the hub genes associated with the treatment of PAH by sivelestat, we employed four algorithms: Degree, MCC, EPC, and CMNC, which allowed us to pinpoint the top 50 targets. Among these, we identified six overlapping

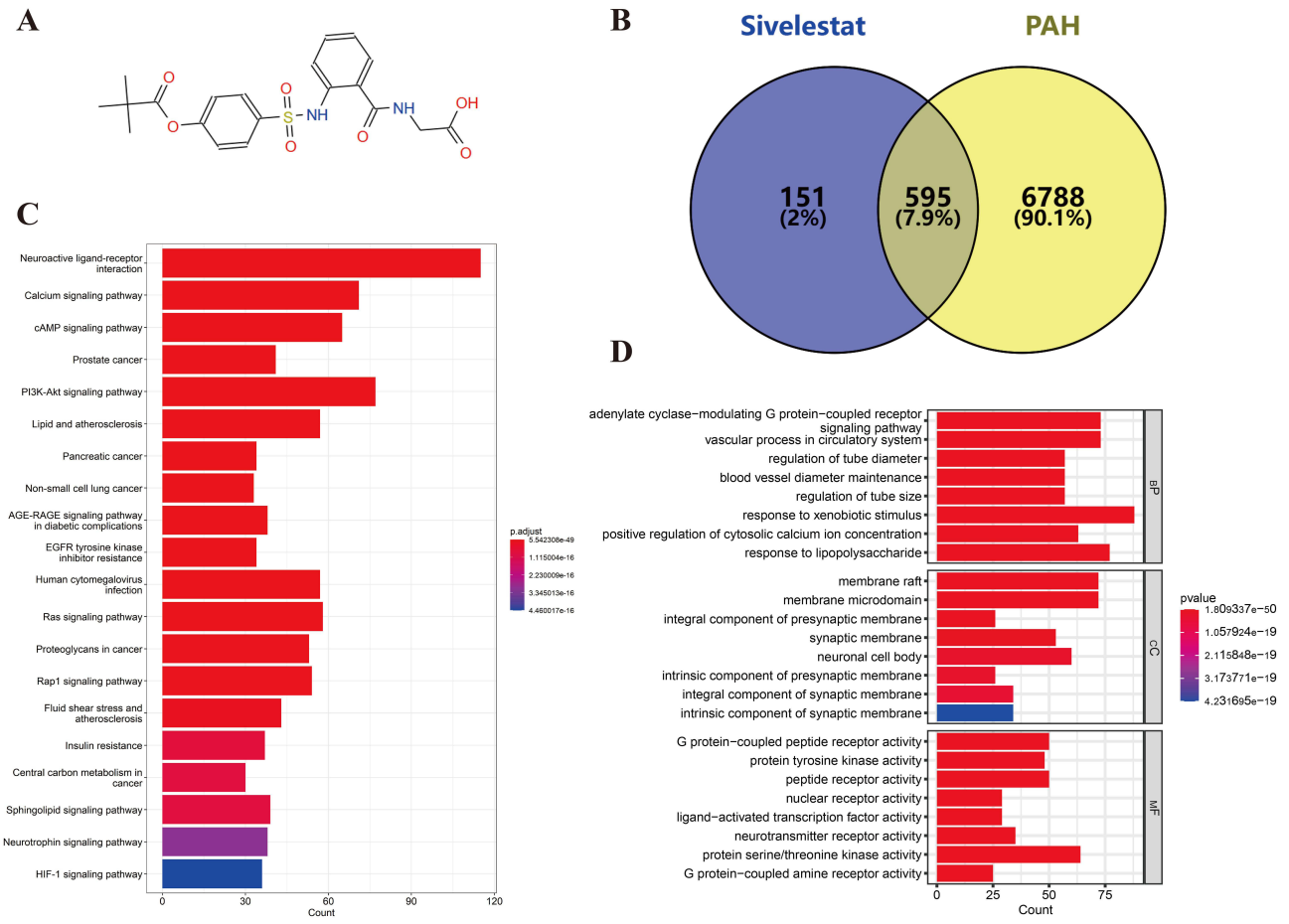

Figure 2 Potential biological targets, functional processes, and signaling pathways of sivelestat in the treatment of PAH. (**A**) The chemical structure of sivelestat. (**B**) Identification of 595 potential targets of sivelestat for PAH treatment through a Venn diagram. (**C**) The top 20 signaling pathways from KEGG enrichment analysis. (**D**) The top 20 biological processes (BP), cellular components (CC), and molecular functions (MF) from GO enrichment analysis.

targets: ERBB2, PTPN2, JAK1, JAK2, PDGFRB, and IGF1R (Figure 3A). These six hub genes are likely to play a significant role in the therapeutic effects of sivelestat on PAH. We retrieved the three-dimensional crystal structures of these hub genes from the PDB database. Subsequently, we utilized Autodock Vina software to conduct molecular docking between the core compound and the target genes, while Pymol software was employed to visualize the docking results and calculate the binding energies. The docking results indicated that the free binding energies exceeded −6.5 kcal/mol, suggesting stable binding interactions. Specifically, the binding energy of ERBB2 with sivelestat was −9.96 kcal/mol (Figure 3B), followed by PTPN2 at −8.81 kcal/mol (Figure 3C), JAK1 at −7.62 kcal/mol (Figure 3D), JAK2 at −9.55 kcal/mol (Figure 3E), PDGFRB at −8.49 kcal/mol (Figure 3F), and IGF1R at −8.77 kcal/mol (Figure 3G).

Sivelestat Administration Alleviates Vascular Remodeling and Alleviates Right Ventricular Hypertrophy in a Hypoxia-Induced PAH

To investigate whether sivelestat can mitigate PAH through its effects on six hub genes, we established a hypoxia-induced PAH model (Figure 4A). Current research suggests that sivelestat exhibits anti-inflammatory and endothelial protective properties.[39,40] Consequently, we analyzed the expression of hub genes in PAECs within the PAH model. The results indicated that the expression levels of ERBB2 and PTPN11 in PAECs remained relatively unchanged, whereas the expression of IGF1R, JAK1, JAK2, and PDGFRB showed significant increases (Figure 4B). We propose that the underlying reason for this phenomenon is that ERBB2 and PTPN11 do not play a critical role in PAECs during the progression of PAH; rather, they may be more relevant in PASMCs or other cell types. Consequently, the endothelial

https://doi.org/10.2147/DDDT.S507240

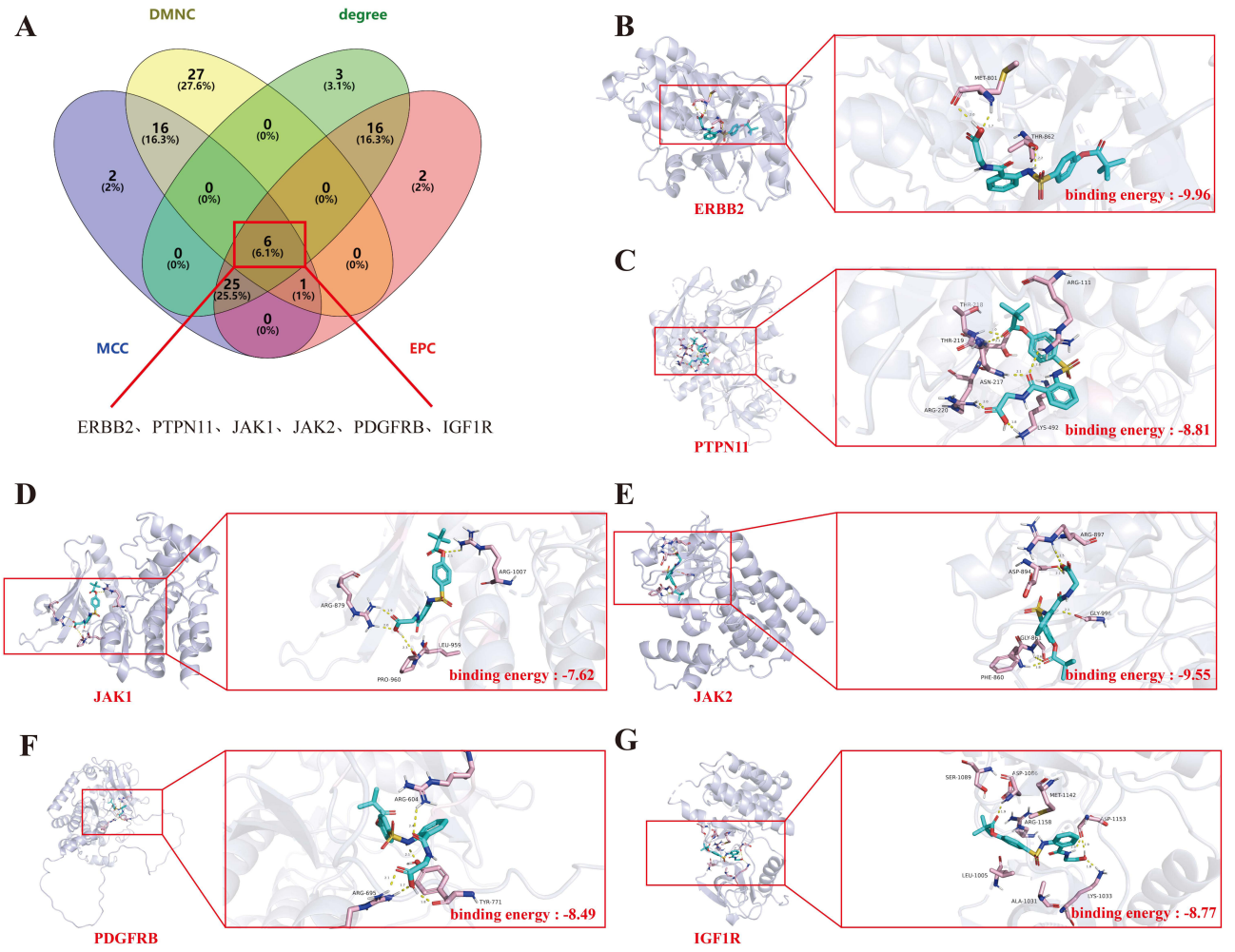

Figure 3 Identification of potential targets of sivelestat for treating PAH using network pharmacology approach. (**A**) The top 50 genes generated by Degree, MCC, EPC, and DMNC algorithms are collected, and overlapping targets are identified as hub genes. (**B**–**G**) Molecular docking is utilized to demonstrate the binding of sivelestat to the hub genes and calculate the corresponding binding energies.

protective effects mediated by sivelestat may be primarily facilitated through IGF1R, JAK1, JAK2, and PDGFRB. To evaluate our hypothesis, we designed the following animal experimental protocol (Figure 4C). The results indicated that, compared to the normoxia group, the blood vessel diameter in the hypoxia group was increased while the lumen was narrowed. At a dosage of 100 mg/kg, sivelestat significantly mitigated the changes in vessel diameter and lumen stenosis (Figure 4D). Similarly, the right ventricle in the hypoxia group exhibited significant enlargement and marked hypertrophy of the cardiomyocytes compared to the normoxia group. Notably, as the concentration of sivelestat increased, there was a significant improvement in right ventricular hypertrophy and a reduction in cardiomyocyte hypertrophy (Figure 4E).

Sivelestat May Alleviate PAH by Modulating the Expression of IGF1R, JAK1, JAK2, and PDFRB

To elucidate the specific mechanisms by which Sivelestat mitigates pulmonary vascular remodeling, we isolated the pulmonary blood vessels from rats across various groups, scraped the vascular intima, and assessed the mRNA and protein expression levels of IGF1R, JAK1, JAK2, and PDFRB. The results indicated that, compared to normoxic conditions, hypoxia significantly increased the mRNA expression of IGF1R, JAK1, JAK2, and PDFRB in PAECs. In contrast, Sivelestat administration markedly decreased the expression levels of these markers (Figure 5A–D). Consistent results were also observed at the protein level (Figure 5E). To accurately evaluate the extent of relief from PAH, we

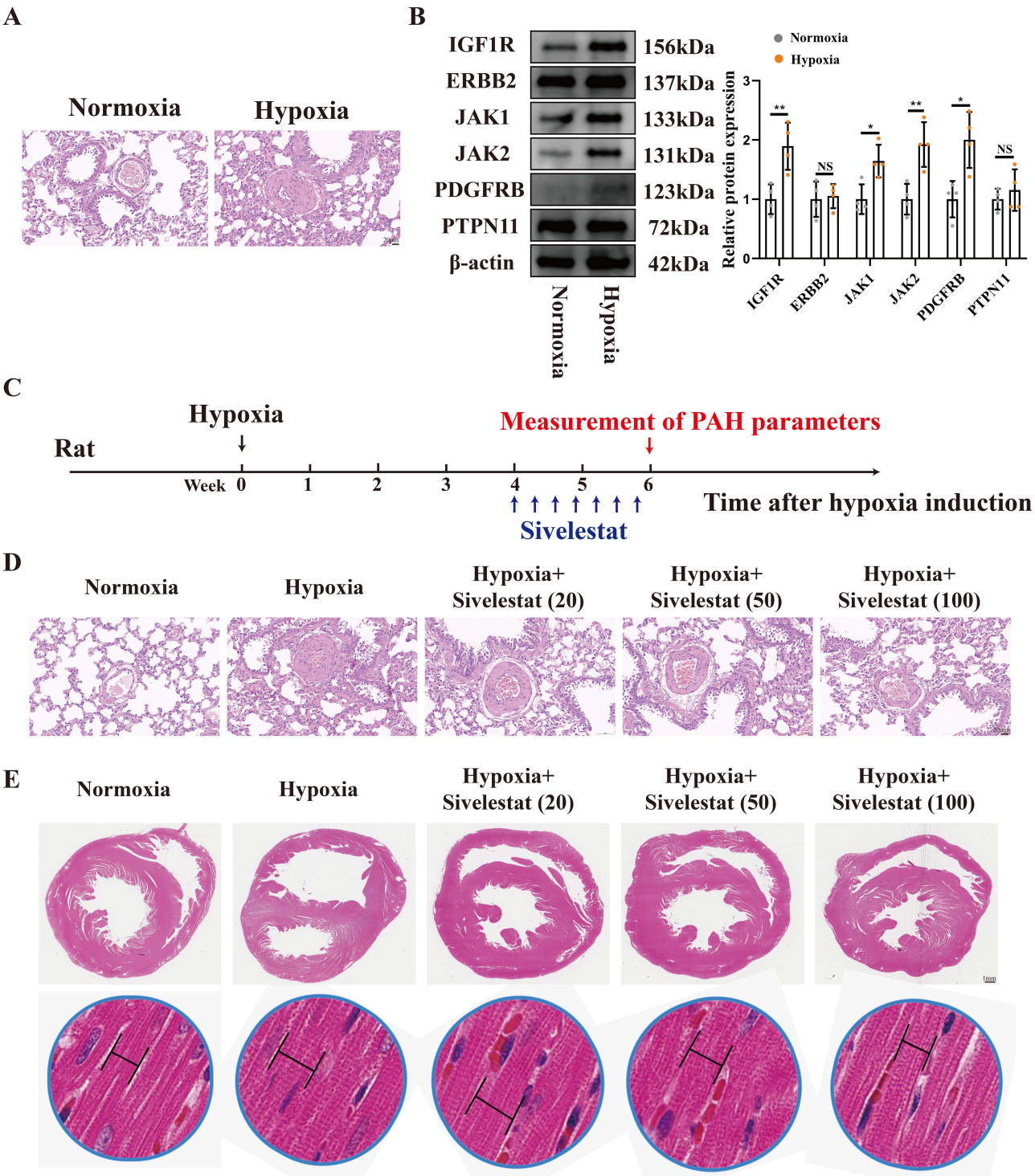

Figure 4 Sivelestat administration alleviates pulmonary vascular remodeling and right ventricular hypertrophy. (**A**) Representative images of pulmonary vessels under hypoxic and normoxic conditions. Bar: 20 μm. (**B**) Expression levels of various proteins in PAECs of rats under hypoxic and normoxic conditions. (**C**) Flowchart of the animal experiment. (**D**) Representative images of pulmonary vessels under different treatment conditions. Bar: 20 μm. (**E**) Slices of the heart under different treatment conditions. Bar: 1 mm. **P* < 0.05, ***P* < 0.01, ****P* < 0.001, ns: No Significance.

measured RVSP. Notably, Sivelestat treatment over two consecutive weeks significantly reduced the hypoxia-induced elevation in RVSP (Figure 5F). We employed WT% to assess vascular remodeling, and similarly, Sivelestat administration improved vascular remodeling outcomes (Figure 5G). Beyond morphological changes, we also investigated

https://doi.org/10.2147/DDDT.S507240

physiological alterations. Our tests on the exercise capabilities of the rats revealed a significant decline in the hypoxic group; however, following Sivelestat treatment, the exercise performance of the rats was notably enhanced (Figure 5H).

Sivelestat Reduces Hypoxia-Induced Proliferation, Migration, and Vascularization of PAECs

Excessive proliferation, migration, and disordered angiogenesis of PAECs are significant contributors to the development of PAH. To further elucidate the mechanism by which sivelestat improves vascular remodeling, we examined the phenotypic changes in PAECs following sivelestat treatment. We employed EDU and CCK8 assays to assess the proliferation capacity of PAECs. The EDU results indicated that a hypoxic environment promoted PAEC proliferation, whereas sivelestat administration mitigated the proliferative effects of hypoxia (Figure 6A). This finding was corroborated by the CCK8 assay (Figure 6B). Additionally, we utilized a Transwell assay to evaluate the migration capability of PAECs. The results demonstrated that hypoxia enhanced PAEC migration, while sivelestat treatment reduced hypoxia-

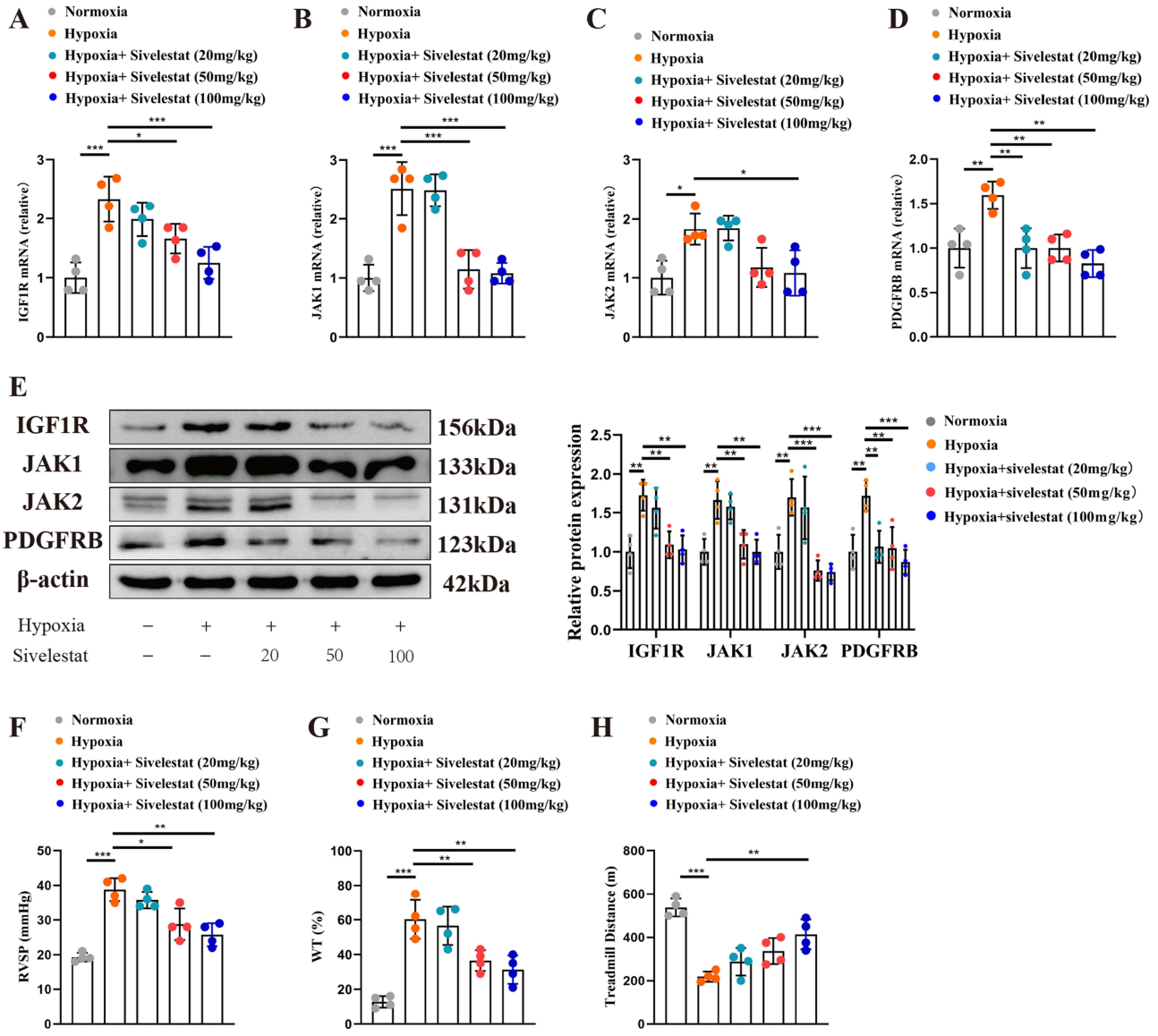

Figure 5 The process of sivelestat administration alleviating PAH. (**A**–**D**) mRNA expression levels of IGF1R, JAK1, JAK2, and PDGFRB in rat pulmonary vascular endothelial cells under different treatment conditions. (**E**) Protein expression levels of IGF1R, JAK1, JAK2, and PDGFRB in rat PAECs under different treatment conditions. (**F**) Right ventricular pressure in rats under different treatment conditions. (**G**) Vascular wall thickness ratio in rats under different treatment conditions. (**H**) Exercise capacity in rats under different treatment conditions. *P < 0.05, **P < 0.01, ***P < 0.001.

https://doi.org/10.2147/DDDT.S507240

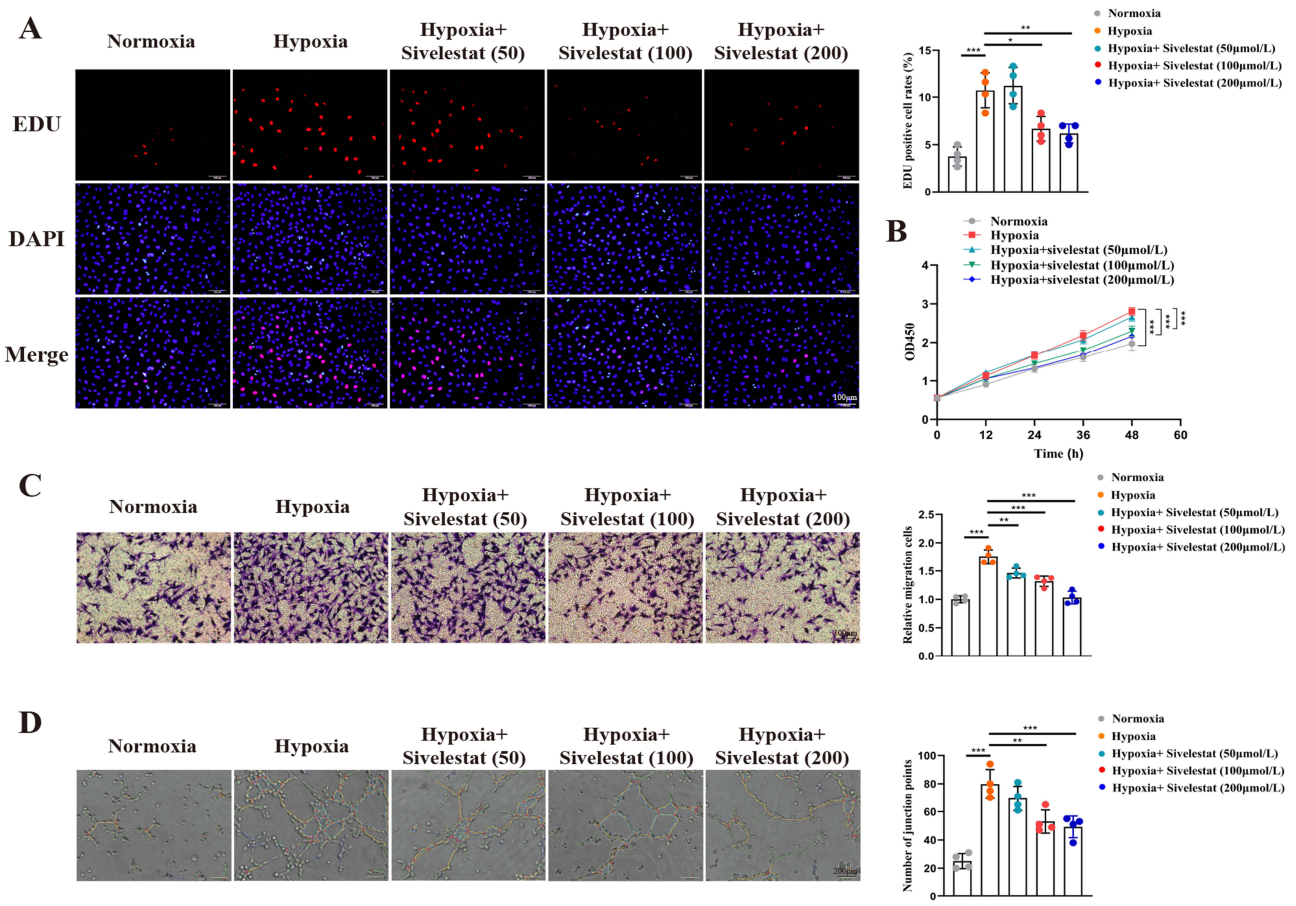

Figure 6 Sivelestat attenuates hypoxia-induced proliferation, migration, and angiogenesis of PAECs. (**A**) The EdU assay was performed to assess the proliferative capacity of PAECs under different treatment conditions, with red indicating proliferating cells and blue indicating nuclei. Bar: 100 μm. (**B**) The CCK8 assay was conducted at different time points to measure cell number under various treatment conditions, and cell proliferation curves were plotted. (**C**) The Transwell assay was employed to evaluate cell migration capacity under different treatment conditions, with a higher cell count indicating stronger migratory ability. Bar: 100 μm. (**D**) Tube formation assay was conducted to assess angiogenic capacity between different groups, with results analyzed using ImageJ software. Bar: 200 μm. **P* < 0.05, ***P* < 0.01, ****P* < 0.001.

induced migration (Figure 6C). Given that the target of sivelestat is closely associated with blood vessel formation (Figure 3D), we further assessed this through experiments focused on vascularization. The results revealed that hypoxia stimulated PAEC vascularization, whereas sivelestat administration significantly inhibited hypoxia-induced vascularization (Figure 6D). To elucidate the critical roles of IGF1R, JAK1, JAK2, and PDGFRB in mediating sivelestat's effects, we overexpressed these targets (Figure S1). We observed that the inhibitory effects of sivelestat on cellular proliferation and migration could be reversed by overexpression of IGF1R, JAK1, JAK2, or PDGFRB. Notably, the suppression of sivelestat's activity was most pronounced following JAK2 overexpression (Figure S2).

Sivelestat Reduces Hypoxia-Induced Proliferation and Migration of PASMCs

Our observations indicate that the histological morphology of pulmonary vascular remodeling reveals that the proliferation and migration of PASMCs are primary factors contributing to luminal stenosis and wall thickening. Consequently, we further investigated the effects of sivelestat on these cells. Results from the EDU experiment demonstrated that hypoxia significantly enhanced the proliferation of PASMCs; however, the administration of sivelestat mitigated this hypoxic effect on cell proliferation (Figure 7A). Supporting this conclusion, CCK8 experiments yielded similar findings (Figure 7B). Furthermore, we assessed the migration capacity of PASMCs using a Transwell assay. The results indicated that hypoxia facilitated the migration of these cells, while sivelestat administration effectively countered this promotional effect (Figure 7C). Furthermore, the inhibitory effects of sivelestat on PASMC proliferation and migration were reversed by overexpression of IGF1R, JAK1, JAK2, or PDGFRB, with JAK2 overexpression exhibiting the most pronounced rescue effect (Figure S3).

https://doi.org/10.2147/DDDT.S507240

Sivelestat Binds to IGF1R, JAK1, JAK2, and PDGFRB

The root-mean-square deviation (RMSD) serves as a robust metric to assess the conformational stability of protein-ligand complexes and quantify positional deviations of atomic coordinates from their initial configurations. Lower RMSD values indicate superior conformational stability. Therefore, RMSD analysis was employed to evaluate the equilibration status of simulated systems. The JAK1-Sivelestat complex achieved equilibrium after 60 ns, stabilizing with RMSD

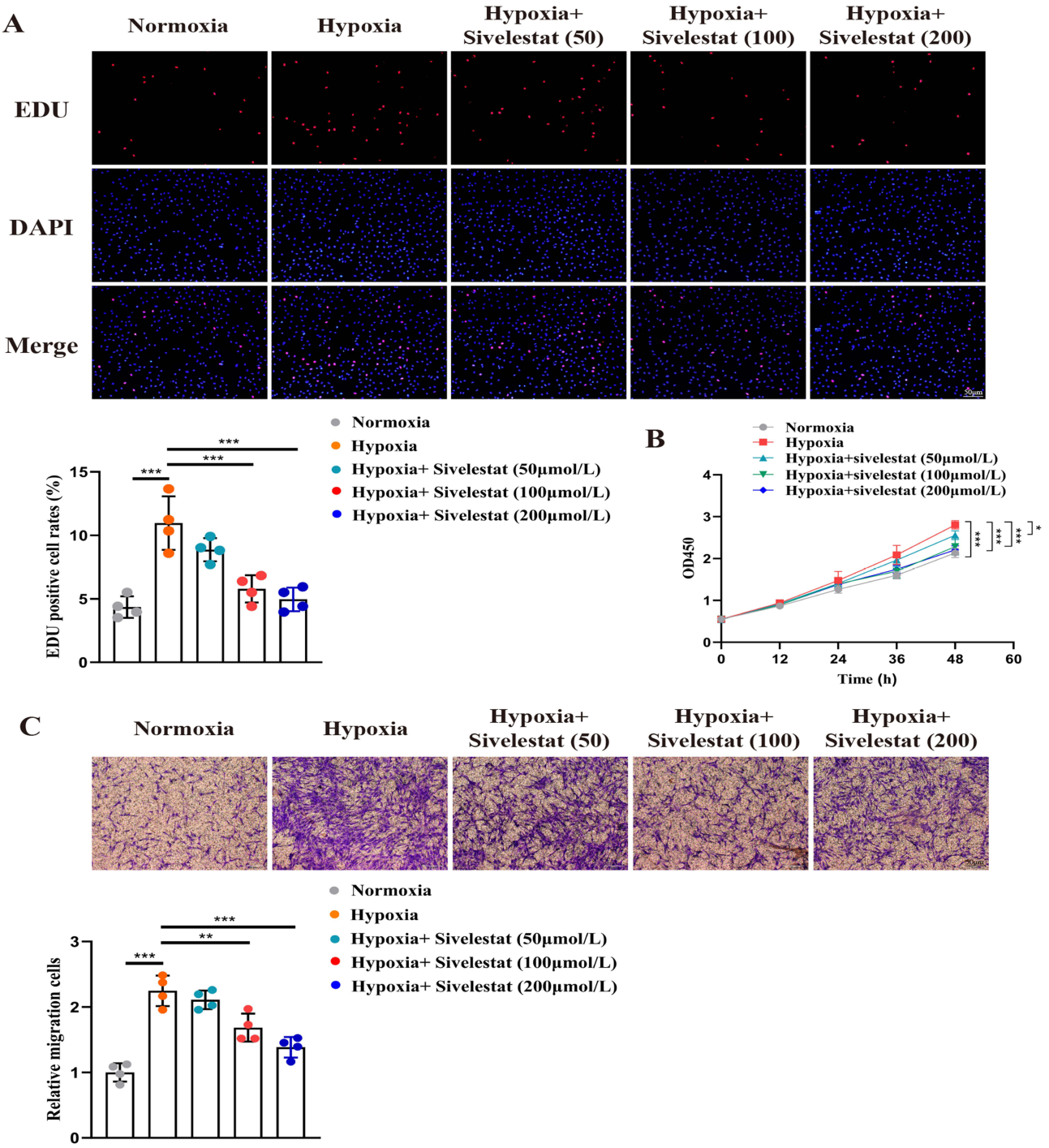

Figure 7 Sivelestat administration reduces hypoxia-induced proliferation and migration of pulmonary arterial smooth muscle cells. (**A**) The EdU assay was performed to assess the proliferative capacity of PASMCs under different treatment conditions, with red indicating proliferating cells and blue indicating nuclei. Bar: 50 μm. (**B**) The CCK8 assay was conducted at different time points to measure cell number under various treatment conditions, and cell proliferation curves were plotted. (**C**) The Transwell assay was employed to evaluate cell migration capacity under different treatment conditions, with a higher cell count indicating stronger migratory ability. Bar: 50 μm. *P < 0.05, **P < 0.01, ***P < 0.001.

 https://doi.org/10.2147/DDDT.S507240

fluctuations around 3.0 Å. The IGF1R-Sivelestat complex reached equilibrium within 20 ns (RMSD ~3.4 Å), while the PDGFRB-Sivelestat system equilibrated after 80 ns (RMSD ~9.4 Å). Notably, the JAK2-JH1-Sivelestat complex demonstrated rapid stabilization within 10 ns (RMSD ~2.9 Å) (Figure S4A). These results collectively indicate strong binding stability between Sivelestat and target proteins (JAK1, IGF1R, PDGFRB, and JAK2).

Further structural analysis revealed minor fluctuations in both radius of gyration (Rg) and solvent-accessible surface area (SASA) values for all complexes during molecular dynamics simulations (Figures S4B-S4C), suggesting conformational adjustments during ligand-protein interactions while maintaining overall structural integrity.

Hydrogen bonding plays a pivotal role in mediating ligand-protein interactions and stabilizing molecular recognition. The dynamic hydrogen bond count between Sivelestat and various protein targets was systematically analyzed throughout molecular dynamics simulations (Figure S4D).

The JAK1-Sivelestat complex exhibited hydrogen bond fluctuations ranging from 0 to 6, with a predominant occupancy of approximately 4 hydrogen bonds throughout the simulation trajectory. Similarly, the IGF1R-Sivelestat system demonstrated hydrogen bond counts varying between 0 and 6, though notably maintaining a higher average of 5 hydrogen bonds in most sampled conformations. More pronounced variability was observed in the PDGFRB-Sivelestat complex, where hydrogen bonds spanned from 0 to 8, yet the predominant interaction state retained approximately 4 hydrogen bonds. The JAK2-JH1-Sivelestat complex displayed an intermediate range of 0–7 hydrogen bonds, with a modal value of 4 hydrogen bonds during productive binding phases.

Root-mean-square fluctuation (RMSF) analysis (Figure S4E) revealed limited residue flexibility across all complexes, with most amino acid residues demonstrating fluctuations below 3.0 Å. This low RMSF profile indicates restricted backbone mobility and enhanced structural stability in the ligand-bound states.

In conclusion, comprehensive molecular dynamics analyses confirm stable binding conformations between Sivelestat and four tyrosine kinase targets (JAK1, IGF1R, PDGFRB, JAK2), characterized by favorable hydrogen-bond interactions, restricted structural fluctuations, and sustained conformational stability. These computational findings strongly support Sivelestat's potential as a multi-target inhibitor through robust molecular recognition mechanisms.

Discussion

In this study, we employed a network pharmacology approach to predict and experimentally validate the potential biological targets, functional processes, and signaling pathways implicated in the treatment of PAH with sivelestat. Furthermore, key biological targets, including IGF1R, JAK1, JAK2, and PDGFRB, were confirmed through experimental validation. Our findings indicate that sivelestat can mitigate PAH by inhibiting the proliferation and migration of PAECs and PASMCs, as well as by improving pulmonary vascular remodeling.

Following the network pharmacology prediction, we identified six hub genes. However, current research indicates that sivelestat plays a significant role in endothelial injury. Consequently, we conducted verification exclusively in PAECs, revealing changes in four genes. We hypothesize that this outcome may be attributed to the fact that not all genes implicated in the development of PAH operate within endothelial cells;[39] they may also influence PAH through pathways involving smooth muscle cells, macrophages, and fibroblasts. This aspect was not explored further, which represents a limitation of our study.

IGF1R is a transmembrane protein that plays a critical role in various cellular processes, including growth and survival.[41] Inhibition of IGF1R has been demonstrated to significantly alleviate PAH in mouse models.[42] Furthermore, it plays a role in the pathogenesis of the disease by modulating the PI3K/AKT/mTOR signaling pathway.[43] Our experiments confirmed the upregulation of IGF1R expression in PAECs in PAH. Notably, the addition of sivelestat was found to inhibit IGF1R expression, suggesting a potential therapeutic mechanism for sivelestat in addressing PAH through IGF1R modulation.

JAK1 and JAK2 are intracellular tyrosine kinases that play pivotal roles in the JAK-STAT signaling pathway, which is crucial for mediating various cellular responses, including inflammation and immune function.[44] Targeting the JAK-STAT signaling pathway has shown promise in improving PAH, as it can modify the pathological processes involved in the disease.[45] Inhibition of JAK1 and JAK2 has been found to prevent fibrosis in the pulmonary vascular bed and alleviate PAH.[46] Our research indicates that both JAK1 and JAK2 are upregulated in hypoxia-induced PAH models.

Furthermore, treatment with sivelestat significantly suppressed the expression of JAK1 and JAK2, suggesting that it may exert beneficial effects in mitigating the progression of PAH through the modulation of JAK-STAT signaling.

PDGFRB is a receptor tyrosine kinase that plays a crucial role in regulating cell proliferation, survival, and vascular remodeling.[47] Research has demonstrated that PDGFRB is instrumental in controlling pulmonary vascular remodeling; blockade of its signaling can significantly alleviate PAH in experimental models.[48] Our findings align with previous studies, revealing that treatment with sivelestat effectively suppresses PDGFRB expression. This suggests that sivelestat may exert beneficial effects on pulmonary hypertension through its interaction with the PDGFRB signaling pathway, potentially contributing to reduced vascular remodeling and improved outcomes.

The identification of IGF1R, JAK1/JAK2, and PDGFRB as hub genes (Figures 2–3) aligns with their established roles in PAH pathogenesis (eg, IGF1R/PASMC proliferation,[42] JAK-STAT signaling in vascular remodeling[49]). Molecular docking and experimental suppression of these targets (Figures 5–7) validate their relevance to sivelestat's mechanism. The observed reduction in RVSP, vascular remodeling, and PAEC/PASMC proliferation/migration (Figures 4–7) directly supports the conclusion that sivelestat ameliorates PAH by targeting hypoxia-driven pathways.

This study presents a significant advantage by integrating network pharmacology with fundamental experiments to thoroughly explore the feasibility of sivelestat for treating pulmonary hypertension. For the first time, we identified sivelestat as a potential therapeutic agent for pulmonary hypertension and unveiled its possible underlying mechanisms. However, this study has limitations, While this study identifies sivelestat's potential in alleviating hypoxia-induced PAH through IGF1R, JAK1/JAK2, and PDGFRB modulation, several limitations warrant consideration. The hypoxia model, though widely used, may incompletely replicate neutrophil elastase-driven inflammatory pathways relevant to PAH. Network pharmacology prioritized druggable targets but excluded canonical PAH genes (eg, BMPR2), and small sample sizes constrain statistical power. While network pharmacology provided a broad framework to identify sivelestat's potential targets in PAH, this approach inherently emphasizes breadth over depth. The study prioritized uncovering multitarget interactions (eg, IGF1R, JAK1/JAK2, PDGFRB) to reflect PAH's multifactorial nature but did not fully elucidate the upstream drivers (eg, transcription factors, kinases) or hierarchical signaling relationships among these targets. Future studies should integrate multi-omics data (eg, transcriptomics, phosphoproteomics) to resolve the mechanistic hierarchy and validate the primary pathways through which sivelestat exerts its therapeutic effects.

Data Sharing Statement

The datasets used and/or analyzed during the current study are available from the corresponding author upon reasonable request.

Ethical Approval

Ethics consent to participate and consent to publish.

The Research Ethics Committee at Jinzhou Medical University granted approval for all animal experiments and methodologies (2022031001). The Laboratory Animal Science Department facilitated the procurement of SD rats. Throughout all experimental processes, strict compliance with the established protocols for the care and use of laboratory animals was upheld. The ethics committee of the First Affiliated Hospital at Jinzhou Medical University approved the study protocol (2024216).

Author Contributions

All authors made a significant contribution to the work reported, whether that is in the conception, study design, execution, acquisition of data, analysis and interpretation, or in all these areas; took part in drafting, revising or critically reviewing the article; gave final approval of the version to be published; have agreed on the journal to which the article has been submitted; and agree to be accountable for all aspects of the work.

Funding

This research received support from the Sichuan Scientific Research Project Program (S23094) alongside the Panzhihua Science and Technology Program (2023ZD-S-11).

Disclosure

The authors declare that they have no competing interests in this work.

References

1. Weatherald J, Hemnes AR, Maron BA, et al. Phenotypes in pulmonary hypertension. *Eur Respir J*. 2024;64(3):2301633. doi:10.1183/13993003.01633-2023
2. Levine DJ. Pulmonary arterial hypertension: updates in epidemiology and evaluation of patients. *Am J Manag Care*. 2021;27:S35–s41. doi:10.37765/ajmc.2021.88609
3. Johnson S, Sommer N, Cox-Flaherty K, Weissmann N, Ventetuolo CE, Maron BA. Pulmonary hypertension: a contemporary review. *Am J Respir Crit Care Med*. 2023;208:528–548. doi:10.1164/rccm.202302-0327SO
4. Olsson KM, Corte TJ, Kamp JC, et al. Pulmonary hypertension associated with lung disease: new insights into pathomechanisms, diagnosis, and management. *Lancet Respir Med*. 2023;11:820–835. doi:10.1016/s2213-2600(23)00259-x
5. Mocumbi A, Humbert M, Saxena A, et al. Pulmonary hypertension. *Nat Rev Dis Primers*. 2024;10:1. doi:10.1038/s41572-023-00486-7
6. Ruopp NF, Cockrill BA. Diagnosis and treatment of pulmonary arterial hypertension: a review. *JAMA*. 2022;327:1379–1391. doi:10.1001/jama.2022.4402
7. Sweatt AJ, Miyagawa K, Rhodes CJ, et al. Severe pulmonary arterial hypertension is characterized by increased neutrophil elastase and relative elafin deficiency. *Chest*. 2021;160:1442–1458. doi:10.1016/j.chest.2021.06.028
8. Aldabbous L, Abdul-Salam V, McKinnon T, et al. Neutrophil extracellular traps promote angiogenesis: evidence from vascular pathology in pulmonary hypertension. *Arterioscler Thromb Vasc Biol*. 2016;36:2078–2087. doi:10.1161/atvbaha.116.307634
9. Bogaard HJ, Aman J. Neutrophil elastase: finding its way from mechanism, via biomarker to treatment target in pulmonary hypertension? *Chest*. 2021;160:1177–1178. doi:10.1016/j.chest.2021.06.068
10. Ren J, Deng G, Li R, et al. Possible pharmacological targets and mechanisms of sivelestat in protecting acute lung injury. *Comp Biology Med*. 2024;170:108080. doi:10.1016/j.compbiomed.2024.108080
11. Lv H, Huang L, Yang X, Zhang C, Yu H, Shang X. The clinical effectiveness of sivelestat in treating sepsis patients with both acute respiratory distress syndrome and septic cardiomyopathy. *J Cardiothorac Surg*. 2024;19:399. doi:10.1186/s13019-024-02835-3
12. Amemori H, Maeda Y, Torikai A, Nakashima M. Sivelestat relaxes vascular smooth muscle contraction in human gastric arteries. *J Physiol Biochem*. 2011;67:589–593. doi:10.1007/s13105-011-0105-3
13. Mackarel AJ, Russell KJ, Brady CS, FitzGerald MX, O'Connor CM. Interleukin-8 and Leukotriene-B 4, but not formylmethionyl leucylphenylalanine, stimulate CD18-independent migration of neutrophils across human pulmonary endothelial cells in vitro. *Am J Respir Cell Mol Biol*. 2000;23:154–161. doi:10.1165/ajrcmb.23.2.3853
14. Hopkins AL. Network pharmacology: the next paradigm in drug discovery. *Nat Chem Biol*. 2008;4:682–690. doi:10.1038/nchembio.118
15. Wang X, Wang Y, Yuan T, et al. Network pharmacology provides new insights into the mechanism of traditional Chinese medicine and natural products used to treat pulmonary hypertension. *Phytomedicine*. 2024;135:156062. doi:10.1016/j.phymed.2024.156062
16. Nogales C, Mamdouh ZM, List M, Kiel C, Casas AI, Schmidt H. Network pharmacology: curing causal mechanisms instead of treating symptoms. *Trends Pharmacol Sci*. 2022;43:136–150. doi:10.1016/j.tips.2021.11.004
17. Wang X, Shen Y, Wang S, et al. PharmMapper 2017 update: a web server for potential drug target identification with a comprehensive target pharmacophore database. *Nucleic Acids Res*. 2017;45(W1). doi:10.1093/nar/gkx374
18. Nickel J, Gohlke BO, Erehman J, et al. SuperPred: update on drug classification and target prediction. *Nucleic Acids Res*. 2014;42(Web Server issue W1). doi:10.1093/nar/gku477
19. Wang X, Shen Y, Wang S. PharmMapper 2017 update: a web server for potential drug target identification with a comprehensive target pharmacophore database. *Nucleic Acids Res*. 2017;45(W1). doi:10.1093/nar/gkx374
20. Yao ZJ, Dong J, Che YJ. TargetNet: a web service for predicting potential drug-target interaction profiling via multi-target SAR models. *J Comput Aided Mol Des*. 2016;30(5):413–424. doi:10.1007/s10822-016-9915-2
21. Stelzer G, Rosen N, Plaschkes I. The GeneCards suite: from gene data mining to disease genome sequence analyses. *Curr Protoc Bioinf*. 2016;54:1.30.1–1.30.33. doi:10.1002/cpbi.5
22. Rappaport N, Twik M, Plaschkes I. MalaCards: an amalgamated human disease compendium with diverse clinical and genetic annotation and structured search. *Nucleic Acids Res*. 2017;45(D1). doi:10.1093/nar/gkw1012
23. Sayers EW, Bolton EE, Brister JR, et al. Database resources of the national center for biotechnology information. *Nucleic Acids Res*. 2022;50(D1). doi:10.1093/nar/gkab1112
24. UniProt Consortium T UniProt: the universal protein knowledgebase. *Nucleic Acids Res*: *Nucleic Acids Res*. 2018;46. 46(5):2699. doi: 10.1093/nar/gkw1099
25. Kahvejian A, Quackenbush J, Thompson JF What would you do if you could sequence everything?. *Nat Biotechnol*. 2008;26(10):1125–1133. doi:10.1038/nbt1494
26. Szklarczyk D, Kirsch R, Koutrouli M, et al. The STRING database in 2023: protein-protein association networks and functional enrichment analyses for any sequenced genome of interest. *Nucleic Acids Res*. 2023;51(D1). doi:10.1093/nar/gkac1000
27. Bader GD, Hogue CW. An automated method for finding molecular complexes in large protein interaction networks. *BMC Bioinformatics*. 2003;4:2. doi:10.1186/1471-2105-4-2
28. Deng JL, Xu YH, Wang G. Identification of potential crucial genes and key pathways in breast cancer using bioinformatic analysis. *Frontiers in Genetics*. 2019;10:695. doi:10.3389/fgene.2019.00695
29. Chin CH, Chen SH, Wu HH, Ho CW, Ko MT, Lin CY. cytoHubba: identifying hub objects and sub-networks from complex interactome. *BMC Systems Biology*. 2014;8(Suppl 4):S11. doi:10.1186/1752-0509-8-s4-s11
30. Shen J, Yu S, Sun X, Yin M, Fei J, Zhou J. Identification of key biomarkers associated with development and prognosis in patients with ovarian carcinoma: evidence from bioinformatic analysis. *J Ovarian Res*. 2019;12:110. doi:10.1186/s13048-019-0578-1

31. Mu H, Chen J, Huang W. OmicShare tools: a zero-code interactive online platform for biological data analysis and visualization. *Imeta*. 2024;3(5). doi:10.1002/imt2.228
32. Eberhardt J, Santos-Martins D, Tillack AF, Forli S AutoDock Vina 1.2.0: new docking methods, expanded force field, and Python Bindings. *J Chem Inf Model*. 2021;61(8):3891–3898. doi:10.1021/acs.jcim.1c00203
33. Ormö M, Cubitt AB, Kallio K, Gross LA, Tsien RY, Remington SJ Crystal structure of the Aequorea victoria green fluorescent protein. *Science*. 1996;273. doi:10.1126/science.273.5280.1392
34. Kim S, Chen J, Cheng T, et al. PubChem 2025 update. *Nucleic Acids Res*. 2025;53(D1). doi:10.1093/nar/gkae1059
35. O'Boyle NM, Banck M, James CA, Morley C, Vandermeersch T, Hutchison GR Open babel: an open chemical toolbox. *J Cheminform*. 2011;3:33. doi:10.1186/1758-2946-3-33
36. Jo S, Kim T, Iyer VG, Im W. CHARMM-GUI: a web-based graphical user interface for CHARMM. *J Comput Chem*. 2008;29:1859–1865. doi:10.1002/jcc.20945
37. Mark P, Nilsson L. Structure and dynamics of liquid water with different long-range interaction truncation and temperature control methods in molecular dynamics simulations. *J Comput Chem*. 2002;23:1211–1219. doi:10.1002/jcc.10117
38. Fei Y, Huang X, Ning F, et al. NETs induce ferroptosis of endothelial cells in LPS-ALI through SDC-1/HS and downstream pathways. *Biomed Pharmacother*. 2024;175:116621. doi:10.1016/j.biopha.2024.116621
39. Harada N, Okajima K, Isobe H. Role of neutrophil elastase in development of pulmonary vascular injury and septic shock in rats. *Shock*. 2008;30:379–387. doi:10.1097/SHK.0b013e3181673e2c
40. Iba T, Kidokoro A, Fukunaga M, Takuhiro K, Yoshikawa S, Sugimotoa K. Pretreatment of sivelestat sodium hydrate improves the lung microcirculation and alveolar damage in lipopolysaccharide-induced acute lung inflammation in hamsters. *Shock*. 2006;26:95–98. doi:10.1097/01.shk.0000223126.34017.d9
41. Gui R, Li W, Li Z, et al. Effects and potential mechanisms of IGF1/IGF1R in the liver fibrosis: a review. *Int J Biol Macromol*. 2023;251:126263. doi:10.1016/j.ijbiomac.2023.126263
42. Sun M, Ramchandran R, Chen J, Yang Q, Raj JU. Smooth muscle insulin-like growth factor-1 mediates hypoxia-induced pulmonary hypertension in neonatal Mice. *Am J Respir Cell Mol Biol*. 2016;55:779–791. doi:10.1165/rcmb.2015-0388OC
43. Liu G, Zhang S, Yang S, Shen C, Shi C, Diao W. CircDiaph3 influences PASMC apoptosis by regulating PI3K/AKT/mTOR pathway through IGF1R. *3 Biotech*. 2023;13:342. doi:10.1007/s13205-023-03739-0
44. Agashe RP, Lippman SM, Kurzrock R. JAK: not just another kinase. *Mol Cancer Ther*. 2022;21:1757–1764. doi:10.1158/1535-7163.Mct-22-0323
45. Yerabolu D, Weiss A, Kojonazarov B, et al. Targeting jak-stat signaling in experimental pulmonary hypertension. *Am J Respir Cell Mol Biol*. 2021;64:100–114. doi:10.1165/rcmb.2019-0431OC
46. Karpov AA, Mihailova AM, Shilenko LA, et al. Inhibition of JAK1,2 prevents fibrotic remodeling of pulmonary vascular bed and improves outcomes in the rat model of chronic thromboembolic pulmonary hypertension. *Int J Mol Sci*. 2022;23(24):15646. doi:10.3390/ijms232415646
47. Andrae J, Gallini R, Betsholtz C. Role of platelet-derived growth factors in physiology and medicine. *Genes Develop*. 2008;22:1276–1312. doi:10.1101/gad.1653708
48. Solinc J, Ribot J, Soubrier F, Pavoine C, Dierick F, Nadaud S. The platelet-derived growth factor pathway in pulmonary arterial hypertension. *Life*. 2022;12:658. doi:10.3390/life12050658
49. Roger I, Milara J, Montero P, Cortijo J. The role of JAK/STAT molecular pathway in vascular remodeling associated with pulmonary hypertension. *Int J Mol Sci*. 2021;22:4980. doi:10.3390/ijms22094980